

Direct observation of Higgs mode oscillations in the pump-probe photoemission spectra of electron-phonon mediated superconductors

A. F. Kemper,^{1,2,*} M. A. Sentef,³ B. Moritz,^{4,5} J. K. Freericks,⁶ and T. P. Devereaux^{4,7}

¹*Department of Physics, North Carolina State University, Raleigh, NC 27695, USA*

²*Lawrence Berkeley National Laboratory, 1 Cyclotron Road, Berkeley, CA 94720, USA*

³*HISKP, University of Bonn, Nussallee 14-16, D-53115 Bonn, Germany*

⁴*Stanford Institute for Materials and Energy Sciences (SIMES),*

SLAC National Accelerator Laboratory, Menlo Park, CA 94025, USA

⁵*Department of Physics and Astrophysics, University of North Dakota, Grand Forks, ND 58202, USA*

⁶*Department of Physics, Georgetown University, Washington, DC 20057, USA*

⁷*Geballe Laboratory for Advanced Materials, Stanford University, Stanford, CA 94305*

Using the non-equilibrium Keldysh formalism, we solve the equations of motion for electron-phonon superconductivity, including an ultrafast pump field. We present results for time-dependent photoemission spectra out of equilibrium which probes the dynamics of the superconducting gap edge. The partial melting of the order by the pump field leads to oscillations at twice the melted gap frequency, a hallmark of the Higgs or amplitude mode. Thus the Higgs mode can be directly excited through the nonlinear effects of an electromagnetic field and detected without any additional symmetry breaking.

PACS numbers:

I. INTRODUCTION

The amplitude, or Higgs mode is deeply intertwined with the historical development of the BCS theory of superconductivity. Although the presence of the Higgs mode is fundamental to superconductivity, it remained elusive for many decades, and its presence and observability is still under debate in many contexts.¹⁻³ Direct observation of the Higgs mode as an oscillation of the superconducting order parameter is difficult with standard methods since it does not couple linearly to electromagnetic fields⁴. It can be observed if it is coexistent with another order, such as a charge density wave⁵⁻⁷, however it is difficult to distinguish from other effects such as phonon splitting due to the secondary order⁷.

More generally, the dynamics of superconductors is a field of study with a long rich history. Until recently, studies were mainly limited to the frequency domain, where measurements are averaged over long times. This changed with the advent of time-resolved spectroscopy, which is performed by exciting the system with an ultrashort pump laser pulse, followed by an equally short probe pulse. These tools have opened a new window into the complex dynamics of superconductors (as well as other ordered phases, e.g. CDW insulators⁸) by performing studies on the gap^{9,10}, collective¹¹, quasiparticle^{12,13}, and interaction dynamics^{14,15,16}.

Theoretical studies of the Higgs mode in the time domain have a longer history than experiments (see e.g. Refs. 17-19). However, the theory is usually done within the context of BCS theory, and more importantly, focuses on single-time dynamics. These neglect important dynamical processes that are present in real materials, including melting of the superconducting order, and relaxation processes, and thus provide a qualitative description at best. Recently, it was shown that a driving field

tuned to a frequency $2\omega = 2\Delta$, twice the superconducting gap, could be used to resonantly excite the amplitude mode in NbN²⁰⁻²², which was confirmed by THz transmission experiments.

In this work, we will show that the amplitude mode can be excited without tuning to a resonance, but rather that it is a fundamental part of the dynamics, and how time- and angle-resolved photoemission spectroscopy (tr-ARPES) can be used to directly observe the amplitude mode, without the need for an additional degree of freedom for the amplitude mode to couple to. The pump pulse perturbs the ordered state, resulting in changes of the effective free energy landscape \mathcal{F} . The minimum in \mathcal{F} is reduced and shifts towards smaller order $|\Delta|$. This goes beyond the linear response regime, where the system is simply perturbed from its equilibrium state without affecting the free energy landscape in which it lives. The non-linear coupling is critical to the excitation of the Higgs mode. After perturbation, oscillations about the new minimum will occur at a frequency of $2|\Delta|$, with subsequent damping and hardening as the system returns to its equilibrium state. These amplitude, or ‘‘Higgs’’, oscillations were observed using tr-ARPES in charge- and spin-density wave systems²³⁻²⁶, as well as cold atomic gases²⁷.

The dynamics of the superconducting order parameter are often studied with a ‘‘quantum quench’’, where one of the physical parameters that make up the superconducting state is changed^{17,19}, resulting in damped oscillations with constant final frequency $2\Delta_\infty$. A similar result was obtained numerically through truncated equation of motion approaches.^{28,29} Here, we go beyond the single-time approaches and directly simulate the pump/probe process in a superconductor by self consistently solving the Gor'kov equations in the time domain. We simulate the pump-probe process using a two-time Green's

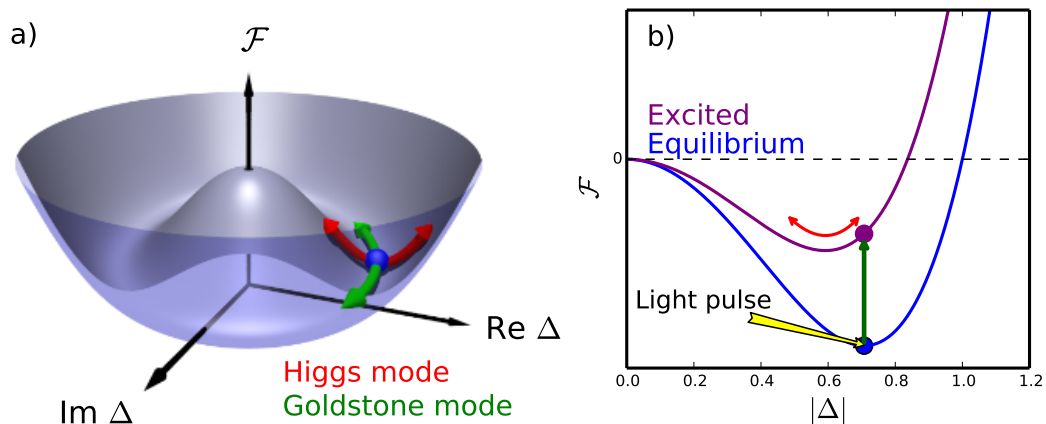


FIG. 1. **Illustration of Higgs excitation** a) Free energy landscape $F[\Delta]$ for the complex order parameter near the phase transition. The Higgs (amplitude) and Nambu-Goldstone (phase) modes are indicated. b) Schematic of the excitation process. The light pulse displaces F on sufficiently short time scales such that the order parameter $|\Delta|$ cannot respond adiabatically leading to oscillations about the new minimum.

function formalism. This formalism captures the full frequency dependence of the pairing interactions the return to equilibrium through electron-phonon scattering, and allows for the calculation of the time-resolved single-particle spectral function, as measured with tr-ARPES³⁰. We focus on the spectra near the Fermi level, where the signatures of the order parameter Δ clearly appear both in and out of equilibrium. After pumping, the system exhibits oscillations at twice the gap energy, which is now time-dependent ($\Delta(t)$). As the pump fluence is increased, the gap partially melts, leading to slower oscillations.

An intuitive understanding of the dynamics that occur during the pump-probe process can be gained by considering the free energy landscape for the complex ($U(1)$) order. The ordered state is perturbed from its equilibrium position by a laser pulse, resulting in changes of the free energy landscape \mathcal{F} . The minimum in \mathcal{F} is reduced due to the decrease of quasiparticles involved in ordering. If the response of the complex order parameter is slower than the changes in \mathcal{F} , oscillations about the new minimum will occur (see Fig. 1) at a frequency of $2|\Delta|$, with subsequent damping and hardening as the system returns to its equilibrium state.

II. METHODS AND MODEL

We consider the Holstein model

$$\mathcal{H} = \sum_{\mathbf{k}} \epsilon(\mathbf{k}) c_{\mathbf{k}}^{\dagger} c_{\mathbf{k}} + \Omega \sum_i b_i^{\dagger} b_i - g \sum_i c_i^{\dagger} c_i (b_i + b_i^{\dagger})$$

where the individual terms represent the kinetic energy of electrons with a dispersion $\epsilon(\mathbf{k})$, the energy of phonons with a frequency Ω , and a coupling between them whose strength is given by g . Here, c_{α}^{\dagger} (c_{α}) are the standard creation (annihilation) operators for an electron in state α ;

similarly, b_{α}^{\dagger} (b_{α}) creates (annihilates) a phonon in state α . For concreteness we study a square lattice dispersion with nearest neighbor hopping (V_{nn}),

$$\epsilon(\mathbf{k}) = -2V_{nn} [\cos(k_x) + \cos(k_y)] - \mu \quad (1)$$

where μ is the chemical potential. We have used the convention that $\hbar = c = e = 1$, which makes inverse energy the unit of time.

The electron-phonon interaction is treated at the self-consistent Born level, where the self-energy is given by

$$\bar{\Sigma}^c(t, t') = ig^2 \bar{\tau}_3 \bar{G}_{\text{loc}}^c(t, t') \bar{\tau}_3 D_0^c(t, t'), \quad (2)$$

where $\bar{\tau}_3$ is the z Pauli matrix in Nambu space, and $\bar{G}_{\text{loc}}^c(t, t') = \sum_{\mathbf{k}} \bar{G}_{\mathbf{k}}^c(t, t')$ i.e. the local Green's function.

The equations to be solved are computationally demanding, and as such the parameters are chosen with an eye towards the feasibility of the simulation. We study a square lattice tight-binding model at half filling. The nearest neighbor hopping strength is $V_{nn} = 0.25$ eV, and the phonon frequency and coupling are chosen as $0.8V_{nn}$ and $1.38V_{nn}$, respectively. The resulting phonon coupling is of intermediate strength ($\lambda \approx 0.58$), which is within the Migdal limit. In the calculations, in addition to the strongly coupled Einstein phonon, to avoid unphysical metastable states within the phonon window due to infinitely long lifetimes we include a weakly coupled low-energy phonon in the distribution with $\Omega_{\text{weak}} = 1$ meV and $g_{\text{weak}}^2 = 1$ meV². For these parameter, the transition temperature $T_c \approx 18.7$ meV. All data shown are calculated at $T = 0.4T_c$.

The pumped superconductor is modeled by self-consistently solving the Gor'kov equations for the Migdal-Eliashberg model in the time domain (see the SI for a detailed discussion). By treating superconductivity at this level, one avoids the issues of gauge invariance that arise in isotropic attractive-U models.^{31,32} The

electron-phonon interactions are treated on the level of the self-consistent Born approximation. The resulting time-domain Green's functions are then used to obtain the tr-ARPES spectra³³.

The solution of the Nambu-Gor'kov equations in the time domain requires self-consistency on the entire Keldysh contour. We utilize the standard two-time Keldysh formalism, where the contour Green's functions are 2x2 matrices in Nambu space^{31,32},

$$\begin{aligned} \bar{G}_{\mathbf{k}}^C(t, t') &= -i \left\langle \mathcal{T}_C \left(\begin{array}{cc} c_{\mathbf{k}\uparrow}(t) c_{\mathbf{k}\uparrow}^\dagger(t') & c_{\mathbf{k}\uparrow}(t) c_{-\mathbf{k}\downarrow}(t') \\ c_{-\mathbf{k}\downarrow}^\dagger(t) c_{\mathbf{k}\uparrow}^\dagger(t') & c_{-\mathbf{k}\downarrow}^\dagger(t) c_{-\mathbf{k}\downarrow}(t') \end{array} \right) \right\rangle \\ &\equiv \begin{pmatrix} G_{\mathbf{k}}^C(t, t') & F_{\mathbf{k}}^C(t, t') \\ F_{\mathbf{k}}^{\dagger C}(t, t') & -G_{-\mathbf{k}}^C(t, t') \end{pmatrix}, \end{aligned} \quad (3)$$

where t and t' lie on the Keldysh contour, and \mathcal{T}_C is the contour time-ordering operator. The equations of motion (on the contour) are

$$\begin{aligned} (i\partial_t \bar{\tau}_0 - \bar{\epsilon}_{\mathbf{k}}(t)) \bar{G}_{\mathbf{k}}^C(t, t') &= \delta^C(t, t') \bar{\tau}_0 \\ &+ \int_C dz \bar{\Sigma}^C(t, z) \bar{G}_{\mathbf{k}}^C(z, t') \end{aligned} \quad (5)$$

$$\bar{\epsilon}_{\mathbf{k}}(t) = \begin{pmatrix} \epsilon_{\uparrow}(\mathbf{k} - \mathbf{A}(t)) & 0 \\ 0 & -\epsilon_{\downarrow}(-\mathbf{k} - \mathbf{A}(t)) \end{pmatrix} \quad (6)$$

where $\bar{\tau}_0$ is the identity matrix, $\epsilon_{\uparrow}(\mathbf{k}) = \epsilon_{\downarrow}(\mathbf{k}) = \epsilon(\mathbf{k})$ is the bare dispersion given above, and $\mathbf{A}(t)$ is the time-varying vector potential in the Hamiltonian gauge. On the Keldysh contour, the Langreth rules can be applied to separate the contour equation into various well-known components: the Matsubara (M), lesser ($<$), and greater ($>$) Green's functions, as well as the mixed real-imaginary $]/[$ types. The equations of motion are solved on the contour by using massively parallel computational methods for integro-differential equations, as described in Ref. 34. The data in the normal state is obtained by performing the simulations without allowing a solution in the anomalous channel.

Once the Green's functions are obtained, time-resolved ARPES (tr-ARPES) spectra can be computed. For a probe pulse of width σ_p , the gauge-invariant tr-ARPES intensity at time t_0 is³³

$$I(\mathbf{k}, \omega, t_0) = \text{Im} \int dt dt' p(t, t', t_0) e^{i\omega(t-t')} G_{\mathbf{k}(t, t')}^<(t, t') \quad (7)$$

where $p(t, t', t_0)$ is a two-dimensional normalized Gaussian with a width σ_p centered at $(t, t') = (t_0, t_0)$. Note that here, only one component of the full Nambu matrix is used. The field-induced shift in \mathbf{k} has to be corrected via a gauge shift in the momentum argument of $G_{\mathbf{k}}^<$ with³⁵

$$\tilde{\mathbf{k}}(t, t') = \mathbf{k} + \frac{1}{t-t'} \int_{t'}^t d\bar{t} \mathbf{A}(\bar{t}). \quad (8)$$

To determine the tr-ARPES spectral weight, we utilize a probe with a Gaussian envelope whose width $\sigma_p = 16.45$ fs.

The field is explicitly included via the Peierls' substitution $\mathbf{k}(t) = \mathbf{k} - \mathbf{A}(t)$, where $\mathbf{A}(t)$ is the vector potential in the Hamiltonian gauge, which has no scalar potential Φ . This includes the field beyond linear coupling, which is critical for the excitation of the Higgs mode (see Ref. 22).

We have checked that the inclusion of local electron-electron scattering up to second order in the interactions does not qualitatively affect our results (a comparison is shown in Sec. IV), where the addition to the self-energy is given by

$$\bar{\Sigma}^C(t, t') = U^2 \bar{\tau}_3 \bar{G}_{\text{loc}}^C(t, t') \bar{\tau}_3 \text{Tr} \{ \bar{G}_{\text{loc}}^C(t, t') \bar{\tau}_3 \bar{G}_{\text{loc}}^C(t', t) \bar{\tau}_3 \}. \quad (9)$$

The phonon bath is kept fixed by ignoring the feedback of the electrons on the phonons; we remain outside of the regime where this is expected to be important, i.e. strong pumping, the formation of static Peierls distortions (CDWs), or quenches of the interaction constant³⁶.

III. RESULTS

Figure 2 shows the tr-ARPES spectra obtained from the calculations in equilibrium (a, b) and after pumping (c). Here, the maximum field strength $E_{\text{max}} = 0.9$ in volts per lattice constant (V/a_0). The spectra are broader than is usual in equilibrium ARPES due to the Heisenberg uncertainty introduced by a time-resolved measurement. The diamond markers indicate the maximum of the constant momentum cut (energy distribution curve or EDC) at $\mathbf{k} = k_F$, which we will denote by ζ throughout. In equilibrium, the spectra show the usual hallmarks of a strongly coupled BCS superconductor: the spectra are pulled back from the Fermi level by some amount, visible both in the decrease of spectral weight at the Fermi level, as well as the downward shift of ζ . In addition, the kink due to the strongly coupled phonon at $\omega = \Omega$ shifts down in binding energy, and shadow bands appear along $\omega = -\epsilon_{\mathbf{k}}$ due to the particle-hole mixing. For the equilibrium superconductor ζ is at roughly -55 meV, although the magnitude of the true gap Δ_0 , which is determined from the spectral gap in the equilibrium self-energy, is slightly less ($\Delta_0 \sim 48$ meV). The difference arises because ζ is shifted by the broadening of the single-particle spectrum and probe resolution.

After pumping, the characteristics of superconductivity are reduced in magnitude. ζ and the gap-shift of the phonon kink are reduced, and the spectral weight in the shadow bands is no longer visible. In fact, the spectrum more closely resembles a normal metal at some elevated temperature. However, superconductivity never fully disappears at this field strength (as we will show below), suggesting that an elevated temperature scenario does not fully capture the behavior here.

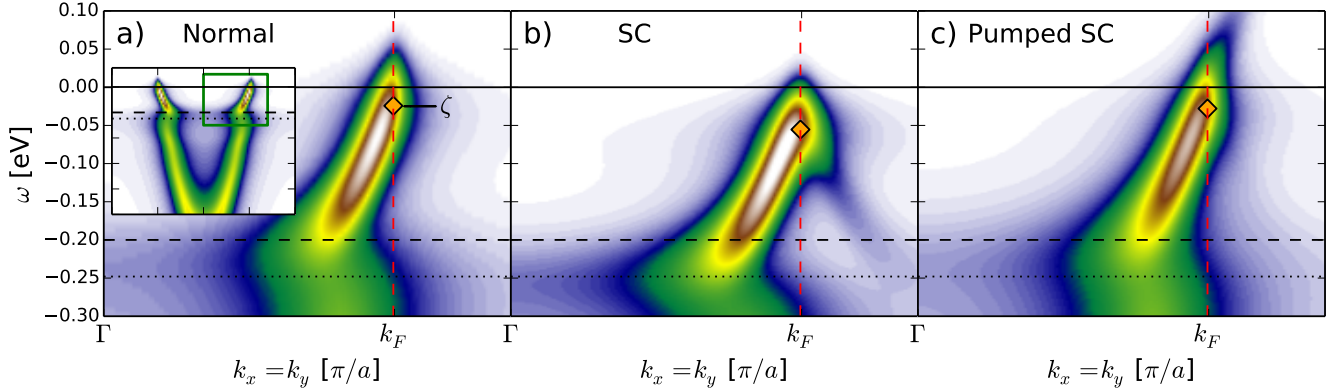


FIG. 2. tr-ARPES spectra of a) the normal state in equilibrium (the inset shows the full spectrum, with the green box indicating the region for panels a-c), b) the superconducting state in equilibrium, and c) the superconducting state, 65.8 fs after a pump with $E_{\max} = 0.9 \text{ V}/a_0$. The vertical red lines indicate the Fermi momentum k_F , the horizontal solid (dashed) line indicates the Fermi level (phonon frequency Ω). The dotted horizontal line indicates the gap-shifted phonon frequency ($\Omega + \Delta_0$). The maximum along the line $\mathbf{k} = k_F$, denoted ζ , is shown with a marker.

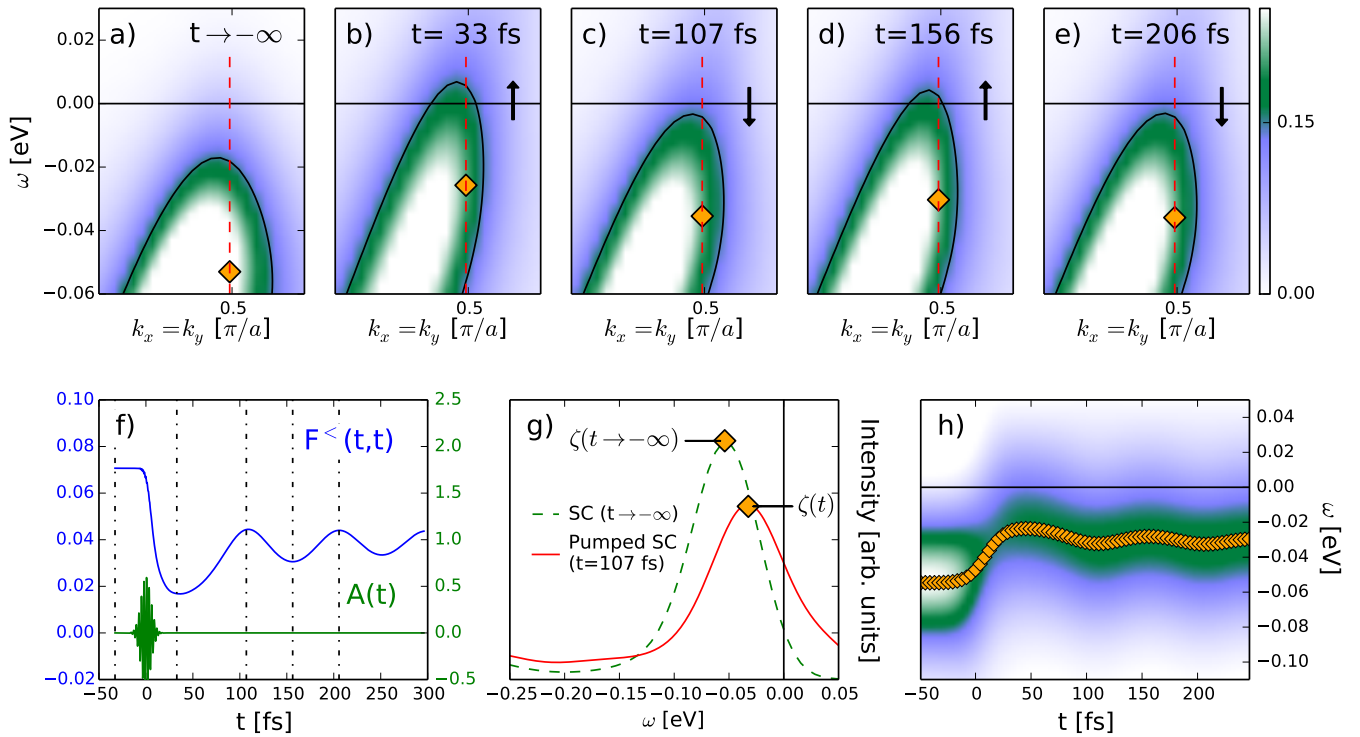


FIG. 3. a) tr-ARPES spectrum near the Fermi level in equilibrium. b)-e) Spectra at various times after the pump, illustrating the shift of the spectral weight back and forth across the Fermi level (a movie is available showing this in detail in the supplementary information). The maximum along the (red) line $\mathbf{k} = k_F$, denoted ζ , is shown with a marker. f) Anomalous density $F^<(t,t)$ (see text), which measures the strength of the superconducting state, and the vector potential $[A(t)]$ as a function of time. The vertical lines indicate the time slices shown in panels a-e). The black arrows indicate the direction of the shift of the spectrum from the previous panel. g) Energy distribution curves (EDCs) at $k = k_F$ (red lines in panels a-e) for equilibrium and pumped superconductor ($t = 107 \text{ fs}$). The marker indicates the EDC maximum (at $\omega = \zeta$). h) False-color plot of EDC intensity as a function of time showing the oscillations after the pump.

We next utilize the strength of the tr-APRES approach and focus on the changes of the spectra near the Fermi level (E_F) where the signature of SC is strongest (Figure 3). The figure shows snapshots of the tr-ARPES spectra before (3a), and after (3b-3e) pumping.

Immediately after the pump (Fig. 3b), there is a shift of spectral weight from lower binding energies to the Fermi level, partially closing the gap, and the EDC center $\zeta(t)$ (\diamond) shifts back towards the Fermi level. The following panels show that the spectral gap first closes right after the pump (3b) and then reopens and closes in the successive time slices (3c-3e), leaving behind a gap which is slightly reduced compared to its equilibrium value (3e). Thus both the spectral intensity as well as the spectral maximum oscillate in time after the pump is applied.

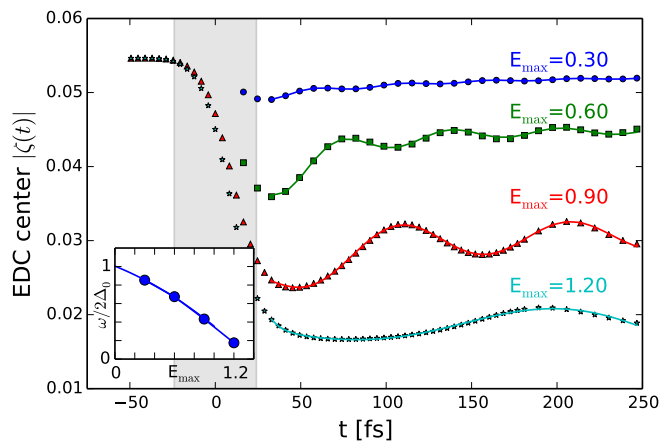


FIG. 4. The position of the EDC maxima ($\zeta(t)$) for various pump fluences. The shaded region indicates the times for which the pump field is on (as defined by 1.5 the field width σ). Solid lines are fits to a decaying exponential plus a damped oscillation. Inset: fitted oscillation frequencies as a function of pump fluence (maximum field in V/a_0). The solid line is a quadratic polynomial fit.

To show that the superconductivity remains even though there is spectral weight in the gap, we consider the “anomalous density” $F^<(t, t) \equiv \sum_{\mathbf{k}} F_{\mathbf{k}}^<(t, t)$ [in analogy with the normal density $n(t) \equiv -i \sum_{\mathbf{k}} G_{\mathbf{k}}^<(t, t)$] shown in panel f. In equilibrium BCS theory, this quantity is related to one side of the gap equation,

$$F_{\mathbf{k}}^<(t, t' = t) = \frac{\Delta_0}{2E_{\mathbf{k}}} \tanh\left(\frac{E_{\mathbf{k}}}{2T}\right), \quad (10)$$

where $E_{\mathbf{k}} = \sqrt{\epsilon_{\mathbf{k}} + \Delta_0^2}$. After pumping, although the magnitude of the order parameter is reduced, superconductivity is still present. Moreover, $F^<(t, t)$ shows the same oscillations as observed in the spectra. The oscillations occur for long times after the pump pulse indicating that they are intrinsic to the superconducting state, rather than directly related to particulars of the pump. The snapshots (panels c-e) are taken at times corresponding to the minima and maxima of the oscillations.

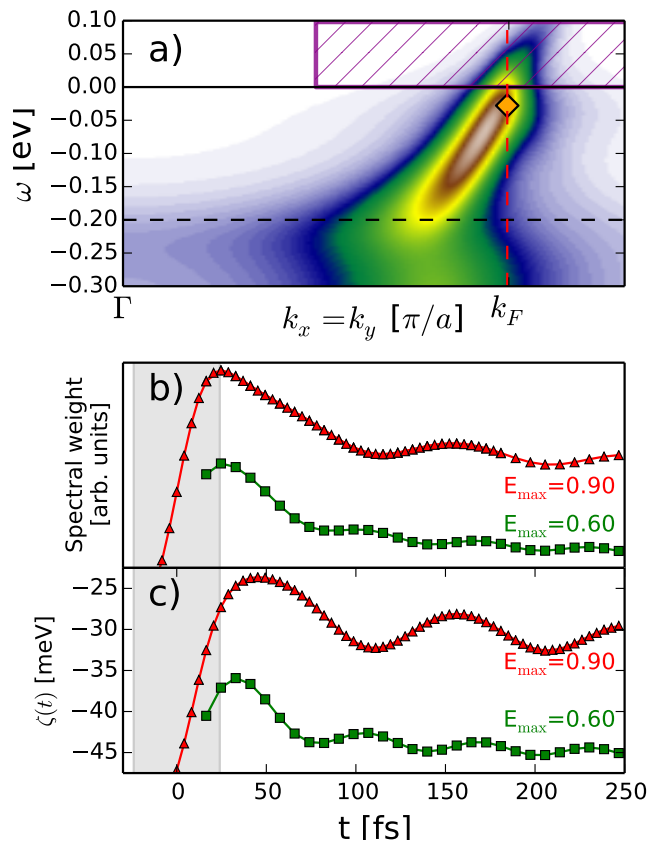


FIG. 5. a) tr-ARPES spectrum in the superconducting state, 65.8 fs after the pump with $E_{\max} = 0.6 V/a_0$. The hatched area indicates the region for integration in panel b), the orange marker the EDC maximum. b) Spectral weight integrated above E_F for two pump fluences (indicated in V/a_0). c) EDC maxima $\zeta(t)$ reproduced from Fig. 4.

We further investigate the oscillations by considering the EDCs at $\mathbf{k} = k_F$ and analyze the dynamics. Figure 3g) shows the EDCs for the equilibrium and pumped superconductor (at $t = 107$ fs). After pumping, ζ returns towards the Fermi level, but not fully. Figure 3h) shows the EDCs as a function of time delay. Upon arrival of the pump, the superconductivity is reduced as spectral weight is scattered to above the Fermi level and across the Brillouin zone. The band subsequently shifts back and forth at a particular frequency. This is markedly different from the normal state, where the spectra after pumping return monotonically to equilibrium³⁰ (unless phonons are resonantly excited or the pump is sufficiently strong³⁶), indicating that the superconducting order is responsible for the oscillations.

By increasing the pump fluence, the order can be further reduced, and the effects of further reduction on the oscillations can be observed. Fig. 4 shows the oscillations after pumping for various pump fluences. With increasing pump fluence, the SC is further suppressed, as reflected in the reduction of $|\zeta|$. Concomitantly with the decrease in SC, the oscillations slow down, confirming

that the mode is determined by the state of the system after pumping. This is the same mechanism that leads to changes in the effective self-energy in the normal state after pumping³⁷, although the field threshold where the system deviates from the equilibrium behavior is much lower. $\zeta(t)$ is fitted to a decaying exponential combined with a damped oscillation. The obtained frequencies ω , scaled by twice the equilibrium gap $2\Delta_0$, are shown in the Figure inset. In the limit of zero fluence, the oscillation frequency ω extrapolates to $2\Delta_0$, the equilibrium gap. This implies that tr-ARPES can provide a clean measurement of Δ_0 , which is obscured in equilibrium by broadening of the spectral function and energy resolution.

The effects of the changing gap at the Fermi level due to amplitude mode oscillations are visible across the entire spectrum, including at the gap edge, at the phonon kink, and above the Fermi level. To illustrate this, we integrate the spectral weight above the Fermi level, where the experimental signal to noise ratio is usually large. Fig. 5 compares the integrated spectral weight (Fig. 5b) with $\zeta(t)$ extracted from the EDCs as before. The oscillations are readily resolvable in both cases, in particular for weaker fields where the early-time behavior is not dominated by simple scattering. To further underscore the point that these oscillations are absent when there is no superconducting condensate, Fig. 6 shows a comparison for similar fields between the superconducting and normal states.

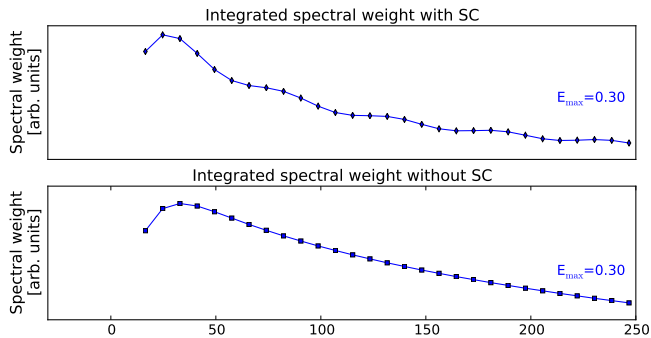


FIG. 6. Spectral weight integrated above E_F for comparing the superconducting and normal states (indicated in V/a_0). The gray region indicates the times where the field is on. The oscillations are only visible when the superconducting order is finite.

IV. EFFECT OF ELECTRON-ELECTRON INTERACTIONS

To account for electron-electron interactions, we have considered local electron-electron scattering (U) at the level of self-consistent second order perturbation theory. The inclusion of electron-electron scattering changes the

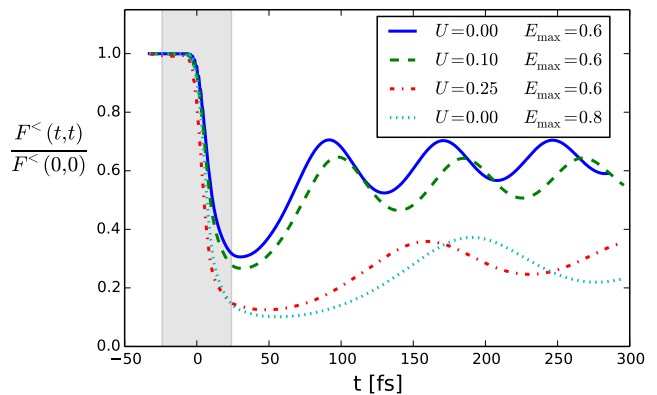


FIG. 7. Normalized “superconducting density” $F^<(t,t)$ (see main text) for various strengths of the Coulomb scattering U . The gray region indicates the times where the field is on. Fields are in units of V/a_0 , and interactions in eV.

energy absorption and thus the state after pumping, leading to a change in the oscillation frequency as the superconducting order is weaker, as illustrated in Fig. 7. For comparison, a data set with larger field but without Coulomb scattering is also shown.

V. CONCLUSION

The results of this study indicate that time-resolved ARPES can be used to directly study the dynamics of Cooper pairs by examining the time-resolved single particle spectral function, making the identification and examination of the Higgs mode available in superconductors. This opens up new avenues for studying superconductivity, both BCS and unconventional. By perturbing the superconducting order from its equilibrium state through nonlinear coupling to a strong field, we can access regions of phase space that are not sampled in equilibrium. This could be particularly interesting in the case where several competing orders are present, such as in the high- T_c cuprates and pnictides.

More generally, the field of pump-probe spectroscopy, and nonlinear coupling to a driving potential, is providing the means to observe phenomena that were previously inaccessible to experiment. Here, we have illustrated this concept in the context of Higgs oscillations in condensed matter, and observations were reported previously in two rather dissimilar systems: NbN ^{21,22}, and cold atomic gases²⁷.

The Higgs mode is just one example of a phenomenon that can be observed or unraveled from others by going into the time domain and perturbing the system far from its equilibrium state. Others include, for example, pumping the lattice and driving the system from the disordered to a (possibly) ordered phase³⁸. Within this context, the combined capability of experiment and theory in non-equilibrium spectroscopy and modeling is set

to grow into a fruitful approach to studying emergent physics.

ACKNOWLEDGMENTS

We would like to thank P. Kirchmann for helpful discussions. A.F.K. was supported by the Laboratory Directed Research and Development Program of Lawrence Berkeley National Laboratory under U.S. Department of Energy Contract No. DE-AC02-05CH11231. B.M and T.P.D. were supported by the U.S. Department of Energy, Office of Basic Energy Sciences, Materials Sci-

ences and Engineering under Contract No. DE-AC02-76SF00515. J.K.F. was supported by the U.S. Department of Energy, Office of Basic Energy Sciences, Materials Sciences and Engineering under Contract No. DE-FG02-08ER46542 and also by the McDevitt bequest at Georgetown. The collaboration was supported by the U.S. Department of Energy, Office of Basic Energy Sciences, Materials Sciences and Engineering under Contract No. de-sc0007091. Computational resources were provided by the National Energy Research Scientific Computing Center supported by the U.S. Department of Energy, Office of Science, under Contract No. DE-AC02-05CH11231.

-
- * akemper@ncsu.edu
- ¹ S. Tsuchiya, R. Ganesh, and T. Nikuni, *Phys. Rev. B* **88**, 014527 (2013), arXiv:1303.3343 [cond-mat.quant-gas].
 - ² D. Pekker and C. M. Varma, *Annual Review of Condensed Matter Physics* **6**, 269 (2015).
 - ³ T. Cea and L. Benfatto, *ArXiv e-prints* (2014), arXiv:1407.6497 [cond-mat.supr-con].
 - ⁴ D. Podolsky, A. Auerbach, and D. P. Arovas, *Physical Review B* **84**, 174522 (2011).
 - ⁵ R. Sooryakumar and M. V. Klein, *Phys. Rev. Lett.* **45**, 660 (1980).
 - ⁶ P. B. Littlewood and C. M. Varma, *Phys. Rev. Lett.* **47**, 811 (1981).
 - ⁷ M. A. Méasson, Y. Gallais, M. Cazayous, B. Clair, P. Rodière, L. Cario, and A. Sacuto, *Physical Review B* **89**, 060503 (2014).
 - ⁸ S. Hellmann, T. Rohwer, M. Kalläne, K. Hanff, C. Sohrt, A. Stange, A. Carr, M. M. Murnane, H. C. Kapteyn, L. Kipp, M. Bauer, and K. Rossnagel, *Nature Communications* **3**, 1069 (2012), 10.1038/ncomms2078.
 - ⁹ M. Beck, M. Klammer, S. Lang, P. Leiderer, V. V. Kabanov, G. N. Gol'tsman, and J. Demsar, *Phys. Rev. Lett.* **107**, 177007 (2011).
 - ¹⁰ C. L. Smallwood, W. Zhang, T. L. Miller, C. Jozwiak, H. Eisaki, D.-H. Lee, and A. Lanzara, *Phys. Rev. B* **89**, 115126 (2014).
 - ¹¹ J. P. Hinton, J. D. Koralek, G. Yu, E. M. Motoyama, Y. M. Lu, A. Vishwanath, M. Greven, and J. Orenstein, *Phys. Rev. Lett.* **110**, 217002 (2013).
 - ¹² R. Cortés, L. Rettig, Y. Yoshida, H. Eisaki, M. Wolf, and U. Bovensiepen, *Phys. Rev. Lett.* **107**, 097002 (2011).
 - ¹³ C. L. Smallwood, J. P. Hinton, C. Jozwiak, W. Zhang, J. D. Koralek, H. Eisaki, D.-H. Lee, J. Orenstein, and A. Lanzara, *Science* **336**, 1137 (2012).
 - ¹⁴ L. Rettig, R. Cortés, H. S. Jeevan, P. Gegenwart, T. Wolf, J. Fink, and U. Bovensiepen, *New Journal of Physics* **15**, 083023 (2013), arXiv:1304.5355 [cond-mat.supr-con].
 - ¹⁵ J. D. Rameau, S. Freutel, L. Rettig, I. Avigo, M. Ligges, Y. Yoshida, H. Eisaki, J. Schneeloch, R. D. Zhong, Z. J. Xu, G. D. Gu, P. D. Johnson, and U. Bovensiepen, *Phys. Rev. B* **89**, 115115 (2014).
 - ¹⁶ W. Zhang, C. Hwang, C. L. Smallwood, T. L. Miller, G. Afeldt, K. Kurashima, C. Jozwiak, H. Eisaki, T. Adachi, Y. Koike, D.-H. Lee, and A. Lanzara, *Nature Communications* **5**, 4959 (2014).
 - ¹⁷ A. F. Volkov and S. M. Kogan, *Soviet Journal of Experimental and Theoretical Physics* **38**, 1018 (1974).
 - ¹⁸ I. O. Kulik, O. Entin-Wohlman, and R. Orbach, *Journal of Low Temperature Physics* **43**, 591 (1981).
 - ¹⁹ E. A. Yuzbashyan, O. Tsypliyatye, and B. L. Altshuler, *Phys. Rev. Lett.* **96**, 097005 (2006).
 - ²⁰ N. Tsuji and H. Aoki, *ArXiv e-prints* (2014), arXiv:1404.2711.
 - ²¹ R. Matsunaga, Y. I. Hamada, K. Makise, Y. Uzawa, H. Terai, Z. Wang, and R. Shimano, *Phys. Rev. Lett.* **111**, 057002 (2013).
 - ²² R. Matsunaga, N. Tsuji, H. Fujita, A. Sugioka, K. Makise, Y. Uzawa, H. Terai, Z. Wang, H. Aoki, and R. Shimano, *Science* **345**, 1145 (2014).
 - ²³ F. Schmitt, P. S. Kirchmann, U. Bovensiepen, R. G. Moore, L. Rettig, M. Krenz, J.-H. Chu, N. Ru, L. Perfetti, D. H. Lu, M. Wolf, I. R. Fisher, and Z.-X. Shen, *Science* **321**, 1649 (2008).
 - ²⁴ L. Perfetti, P. A. Loukakos, M. Lisowski, U. Bovensiepen, M. Wolf, H. Berger, S. Biermann, and A. Georges, *New Journal of Physics* **10**, 053019 (2008).
 - ²⁵ C. Rüegg, B. Normand, M. Matsumoto, A. Furrer, D. F. McMorrow, K. W. Krämer, H.-U. Güdel, S. N. Gvasaliya, H. Mutka, and M. Boehm, *Physical Review Letters* **100**, 205701 (2008).
 - ²⁶ R. Yusupov, T. Mertelj, V. V. Kabanov, S. Brazovskii, P. Kusar, J.-H. Chu, I. R. Fisher, and D. Mihailovic, *Nature Physics* **6**, 681 (2010).
 - ²⁷ M. Endres, T. Fukuhara, D. Pekker, M. Cheneau, P. Schauß, C. Gross, E. Demler, S. Kuhr, and I. Bloch, *Nature* **487**, 454 (2012).
 - ²⁸ T. Papenkort, V. M. Axt, and T. Kuhn, *Phys. Rev. B* **76**, 224522 (2007).
 - ²⁹ T. Papenkort, T. Kuhn, and V. M. Axt, *Phys. Rev. B* **78**, 132505 (2008).
 - ³⁰ M. Sentef, A. F. Kemper, B. Moritz, J. K. Freericks, Z.-X. Shen, and T. P. Devereaux, *Phys. Rev. X* **3**, 041033 (2013).
 - ³¹ A. Abrikosov, L. Gorkov, and I. Dzyaloshinski, *Methods of Quantum Field Theory in Statistical Physics* (Dover Publications, Inc., 1963).
 - ³² J. Rammer, *Quantum Field Theory of Non-equilibrium States* (Cambridge University Press, 2007).
 - ³³ J. K. Freericks, H. R. Krishnamurthy, and T. Pruschke, *Phys. Rev. Lett* **102**, 136401 (2009).

- ³⁴ G. Stefanucci and R. van Leeuwen, *Nonequilibrium Many-Body Theory of Quantum Systems: A Modern Introduction* (Cambridge University Press, New York, 2013).
- ³⁵ V. Turkowski and J. K. Freericks, *Nonequilibrium dynamical mean-field theory of strongly correlated electrons*, in: *Strongly Correlated Systems: Coherence and Entanglement*, edited by J. M. P. Carmelo, J. M. B. L. dos Santos, V. R. Vieira, and P. D. Sacramento (World Scientific, 2007: 187–210, 2007).
- ³⁶ Y. Murakami, P. Werner, N. Tsuji, and H. Aoki, ArXiv e-prints (2014), arXiv:1407.8288.
- ³⁷ A. F. Kemper, M. A. Sentef, B. Moritz, J. K. Freericks, and T. P. Devereaux, *Physical Review B* **90**, 075126 (2014).
- ³⁸ R. Mankowsky, A. Subedi, M. Först, S. O. Mariager, M. Chollet, H. T. Lemke, J. S. Robinson, J. M. Glownia, M. P. Minitti, A. Frano, M. Fechner, N. A. Spaldin, T. Loew, B. Keimer, A. Georges, and A. Cavalleri, *Nature (London)* **516**, 71 (2014), arXiv:1405.2266 [cond-mat.suprcon].